Journal of Basic Sciences and Artificial Intelligence (JBSAI)

DOI: 10.65098/jbsai.01.2026.53.61

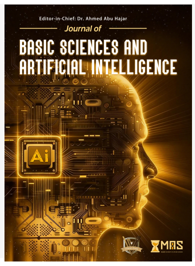

RESEARCH ARTICLE

Hybrid Type-1 and Type-2 Fuzzy Logic Control of Flexible Underwater Robots

Abdul Fattah Jamali*, Hassan Al-Naddaf, Bassem Fares

Department of Control and Automation Engineering, Faculty of Electrical and Electronics Engineering, University of Aleppo, Aleppo 12212, Syria
****Corresponding Author Email: jamali@al-shamal.edu.sy***

ARTICLE DETAILS

Article History:

Received: 07 Jun 2026
Accepted: 11 Sep 2026
Available online: 16 Sep 2026

Online Article Code

ABSTRACT

In this research paper, a mathematical analysis and dynamical comparison have been performed between the Type-1 and Interval Type-2 Fuzzy Sliding Mode Control (IT2-FSMC) frameworks for an underactuated flexible-link underwater robot. Although the Type-1 Fuzzy Sliding Mode Control (Type-1 FSMC) controller ensures stability and satisfactory trajectory tracking ability, the efficiency decreases tremendously whenever the underwater robot encounters severe disturbances of the hydrodynamic nature and uncertainties of up to 50% of the nominal values, causing high-frequency chattering issues and resonant control spillover problems in the flexible links. In order to overcome this basic limitation of the control framework, the nonlinear control policy based on the IT2-FSMC scheme is formulated and designed, which exhibits better mathematical ability to cover the uncertainties with its Footprint of Uncertainty. Through numerical simulations under the effect of constant ocean currents, dry Coulomb friction force, and severe 50% parameter uncertainties, it is evident from the results that the proposed IT2-FSMC controller outperforms the Type-1 one in overcoming all kinds of problems and disturbances.

KEYWORDS

Interval Type-2 Fuzzy Sliding Mode Control; Type-1 Fuzzy Sliding Mode Control; Flexible-Structure Underwater Robot; Extreme Uncertainty; Chattering Suppression; Dynamic Vibration Damping

1. INTRODUCTION

When considering contemporary marine engineering and diving exploratory operations, Autonomous Underwater Vehicles with underwater manipulators are essential tools required to perform complicated and dangerous jobs, such as maintenance of pipelines and inspections of offshore oil facilities (Fossen, 2021). The typical designs of such manipulators imply rigid and heavy constructions that are needed for positioning precision purposes; but at the same time, this construction restricts the operation significantly in terms of high power consumption, high hydrodynamic drag, and poor payload-to-weight ratio (Mendel, 2017). In order to improve these properties, flexible-link manipulators are a promising choice, providing energy efficiency and hydrodynamic advantages (Utkin et al., 2009).

At the same time, control of flexible manipulators is a very complicated problem both theoretically and practically. From a dynamical point of view, it is a highly coupled and underactuated nonlinear mechanical system when the number of degrees of freedom (including vibration modes) is higher than the number of actuators (Slotine & Li, 1991). This creates a dual task for the controller-it should provide correct tracking of the joint trajectory while performing effective vibration damping in order to prevent non-minimum phase behavior (Spong et al., 2020).

Such problems become highly pronounced for open aquatic environments, which experience extremely high uncertainties due to the unpredictable nature of the ocean currents, dry Coulomb friction in the joint seals, and changes in the added mass matrix according to varying payload (Nie & Tan, 2008). In traditional approaches, classic Sliding Mode Control (SMC) is highly resilient against external perturbations; yet, the high-frequency chattering becomes apparent owing to the harsh switching functions used in SMC systems. In flexible structures, this introduces resonant energy, leading to excitation of unmodeled modes and thus resulting in structural collapse or a control spillover effect (Wang et al., 2022).

In order to address the above issue, the Type-1 Fuzzy SMC (Type-1 FSMC) was proposed, which helped to smooth out the switching signal and eliminate the problem of chattering under normal operating conditions (Li et al., 2022). Nonetheless, recent research shows that the effectiveness of the Type-1 approach drops dramatically once the disturbances and parametric uncertainties exceed 50% of nominal values. The reason lies in the fact that crisp membership functions cannot model linguistic and mathematical uncertainties of such a harsh environment (Zhang et al., 2023).

Taking into consideration the above, the following paper introduces a sophisticated control technique called the Hybrid Control System with IT2 Fuzzy SMC (IT2-FSMC). Thanks to the concept of the ”Footprint of Uncertainty” (FOU), this controller gains extra degrees of freedom, making it very robust to serious parametric uncertainties and hydrodynamic disturbances (Fossen & Sørensen, 2023). The purpose of this work is to compare, through mathematical modeling and dynamic simulation, the performance of the IT2-FSMC controller compared to others in terms of its ability to give a smooth and chatter-free control signal while ensuring accuracy and vibration reduction despite uncertainty levels up to 50%.

2. MATHEMATICAL MODELING OF THE FLEXIBLE UNDERWATER ROBOT

In order to design a reliable and robust controller, it is very important to come up with an exact mathematical model for the flexible structure of the underwater robotic arm using the Euler-Lagrange approach. Figure 1 shows the architecture of the investigated system, in which an underactuated Remotely Operated Vehicle (ROV) works in a global coordinate system (X_0, Y_0) in the presence of hydrodynamic disturbances (τ_d) as well as active propulsion/dive forces.

In order to represent the highly coupled kinematics of the investigated

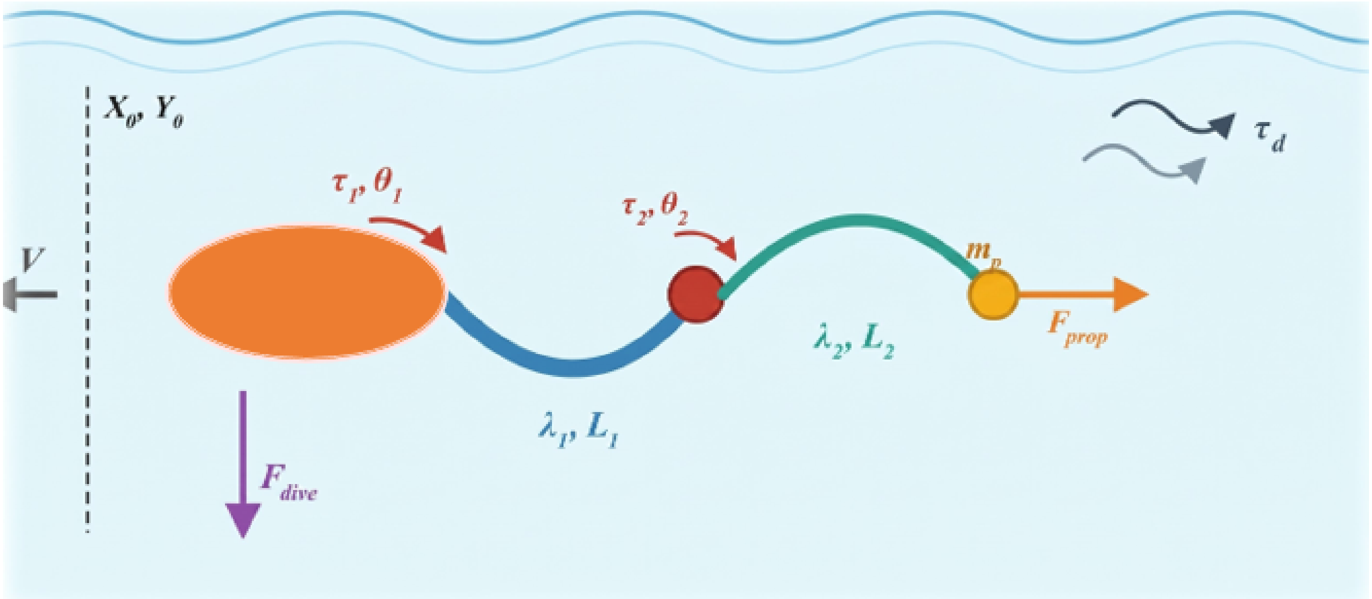

Figure 1 Schematic Diagram of the Flexible Structure of the Underwater Robot (ROV). It showing the global coordinate system (X_0, Y_0), active thruster forces $(F_{prop}, F_{dive}$, joint control torques (τ_1, τ_2), and hydrodynamic disturbances (τ_d)

flexible structure system, Figure 2 provides more information about the body-fixed moving frame (x_i, y_i) of each link. The dynamic state vector (X) of the system is provided in order to consider joint angles (θ_1, θ_2), elastic deformations (λ_1, λ_2) as well as vertical heave motion $(z, \dot{z})$:

$$X = \left[\theta_1, \dot{\theta_1}, \theta_2, \dot{\theta_2}, \lambda_1, \dot{\lambda_1}, \lambda_2, \dot{\lambda_2}, z, \dot{z}\right]^T$$

The absolute position vectors of any arbitrary point along the first and second flexible links are derived relative to these body-fixed frames. Let $r_1\,(x_1, t)$ and $r_2\,(x_2, t)$ be the absolute position vectors. For a mass element dm_1 located at a distance x_1 on the first link, the position vector is given by:

$$r_1\,(x_1, t) : r_1\,(x_1, t) = \begin{bmatrix} x_1 \cos(\theta_1) - \phi_1\,(x_1)\,\lambda_1\,(t) \sin(\theta_1) \\ x_1 \sin(\theta_1) + \phi_1\,(x_1)\,\lambda_1\,(t) \cos(\theta_1) \end{bmatrix} \quad (1)$$

If the links undergo deformations, then phi's represent the mode shapes (eigenfunctions) of the corresponding links, and lambda's are amplitudes of the deformation which depend on the applied external forces. Same thing, we can calculate the position vector for a mass element dm_2 on the second link. Since the second link is attached to the end of the first one, the displacement of that point is also affected by the first link's motions (the combined displacement is equal to L_1 the length of the first link).

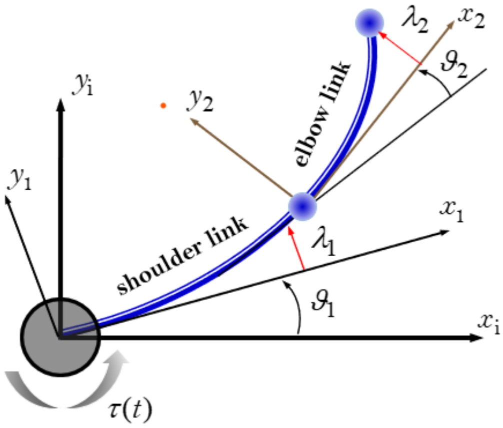

Figure 2 Detailed Kinematic Diagram of the Dual-Link Flexible Manipulator. It shows the body-fixed moving reference frames $(x_1, y_1$ and $x_2, y_2)$, the rigid joint angular coordinates $(\vartheta_1, \vartheta_2)$, and the corresponding transverse elastic deformation displacements (λ_1, λ_2)

$$r_2\,(x_2, t) = r_1\,(L_1, t) + \begin{bmatrix} x_2 \cos(\theta_1 + \theta_2) - \phi_2\,(x_2)\,\lambda_2\,(t) \sin(\theta_1 + \theta_2) \\ x_2 \sin(\theta_1 + \theta_2) + \phi_2\,(x_2)\,\lambda_2\,(t) \cos(\theta_1 + \theta_2) \end{bmatrix} \quad (2)$$

An analytical expression of the dynamic equation for the flexible arm has been derived by a careful energy analysis that incorporates not only the kinetic energy of the system altogether but also the individual parts, as well as the elastic potential energy, if any, of the links. That's why the overall dynamical equation of a flexible arm, based entirely on energy considerations and with the potential and kinetic energy as the two driving elements of the system, is represented as:

$$M\,(q)\,\ddot{q} + C\,(q, \dot{q})\,\dot{q} + D_{arm}\dot{q} + K_{arm}q = \tau + \tau_{current} - \tau_{friction} \quad (3)$$

In parallel, the vertical heave movements of the ROV base, which must remain stable despite the reaction forces generated by the arm, are governed by Newton-Euler equations:

$$m_{total}\ddot{z} = F_z + F_{dz} - d_z\dot{z} - W_B \quad (4)$$

The variables used are: m_{total} is the total mass of the ROV and its payload, F_z is the control input thrust, d_z is the hydrodynamic damping factor, and W_B is the net effective weight. Assuming that the underwater manipulator works in a horizontal plane with the total weight balanced by the buoyancy force, the potential energy U will be mainly due to the elastic strain energy from bending the lightweight links. According to Euler-Bernoulli beam theory, the expression of this potential energy can be written as:

$$U = \frac{1}{2}\sum_{i=1}^{2}\sum_{0}^{L_i} E_i I_i \left(\frac{\partial^2 w_i\,(x_i, t)}{\partial x_i^2}\right)^2 dx_i \quad (5)$$

One of the main things to understand from this description is that the time-varying deformation degrees of freedom (λ_1, λ_2) are dynamic state variables rather than constant parameters. The Lagrangian derivative applied on potential energy of the system by first substituting modal approximation $w_i\,(x_i, t) = \phi_i\,(x_i)\,\lambda_i\,(t)$ will bring out a new set of time-varying equations which will describe the dynamical behavior of the system.

The stiffness matrix of the structure $K_{arm} \in \mathbb{R}^{4\times4}$is computed mathematically from the material properties that have been obtained by experience:

$$K_{arm} = \mathrm{diag}\left(00E_1 \sum_{0}^{L_1} \left(\phi_1'\right)^2 dx_1, E_2 \sum_{0}^{L_2} \left(\phi_2'\right)^2 dx_2 \right) \tag{6}$$

The two zero terms represent the rigid joint coordinates that do not have any elastic potential energy. These mechanical properties have been implemented properly in the 3D Simscape Multibody simulation environment, which has resulted in a stiffness coefficient of $K_{flex_1} = 0.9084$ and $K_{flex_2} = 18.7325$.

2.1 Coupled Inertia Matrix M(q)

After explaining the mathematical expression, some important physical constants related to the flexible underwater arm are introduced: $m_i l_i lc_i$: the mass, the overall length, and the position of the barycenter of link $i\,(i = 1, 2)$.

Ih_i: inertial moment of the joint drive motors.

m_p: mass of the load carried by the gripper.

ρ_i: mass distributed along the flexible member per unite of length.

$\phi_{ij}\,(x)$: the shape of deformation that is supposed to be a combination of mode shapes.

The inertia matrix $M\,(q) \in \mathbb{R}^{4\times4}$ of the whole system that includes the inertia effects of the manipulator's flexibility and of any payload, has also been calculated. This was done by taking into consideration physical parameters and applying some methods. The equations were simplified by grouping physically related terms into a new mathematical description called the dynamic parameter vector $(\alpha_k, k = 1, 2 \ldots 23)$.

The whole inertia mass matrix elements are presented in the form of:

$$m_{11} = \alpha_1 + \alpha_2 \cos(\theta_2) - (\alpha_3\lambda_1 + \alpha_4\lambda_2)\sin(\theta_2) \tag{7}$$

$$m_{12} = m_{21} = \alpha_5 + \alpha_6 \cos(\theta_2) + (\alpha_7\lambda_1 + \alpha_8\lambda_2)\sin(\theta_2) \tag{8}$$

$$m_{13} = m_{31} = \alpha_9 + \alpha_{10}\cos(\theta_2) - \alpha_{11}\lambda_2 \sin(\theta_2) \tag{9}$$

$$m_{14} = m_{41} = \alpha_{12} + \alpha_{13}\cos(\theta_2) - \alpha_{14}\lambda_1 \sin(\theta_2) \tag{10}$$

$$m_{22} = \alpha_{15} \tag{11}$$

$$m_{23} = m_{32} = \alpha_{16} + \alpha_{17}\cos(\theta_2) - (\alpha_{18}\lambda_1 + \alpha_{19}\lambda_2)\sin(\theta_2) \tag{12}$$

$$m_{24} = m_{42} = \alpha_{20} \tag{13}$$

$$m_{33} = \alpha_{21}, \quad m_{34} = m_{43} = \alpha_{22}, \quad m_{44} = \alpha_{23} \tag{14}$$

2.2 Coriolis and Centrifugal Force Vectors $C\,(q,\dot{q})$

To ensure mathematical rigor and the conservation of energy, the Coriolis and centrifugal force vectors are deterministically derived from the inertia matrix $M\,(q)$ using Christoffel symbols of the first kind:

$$c_{ijk} = \frac{1}{2}\left(\frac{\partial m_{ij}}{\partial q_k} + \frac{\partial m_{ik}}{\partial q_j} - \frac{\partial m_{jk}}{\partial q_i}\right) \tag{15}$$

The explicit elements are formulated using a corresponding set of lumped parameters $\beta_k\ (k = 1, 2, \ldots, 16)$:

$$\begin{aligned} c_1 = &-\beta_1\dot{\theta}_2 + \beta_2\dot{\lambda}_1 + \beta_3\dot{\lambda}_2\dot{\theta}_2 + \beta_4\dot{\theta}_2 + \beta_5\dot{\lambda}_1 + \beta_6\dot{\lambda}_2\dot{\theta}_1 \\ &+ \beta_7\lambda_1\lambda_2\sin(\theta_2) \end{aligned} \tag{16}$$

$$\begin{aligned} c_2 = &\ \beta_4\dot{\theta}_1 + \beta_8\lambda_1\dot{\theta}_1\sin(\theta_2) + \beta_9\dot{\lambda}_2 + \beta_{10}\lambda_1\dot{\theta}_1 \\ &+ \beta_{11}\left(\lambda_1^2\dot{\lambda}_2 + \dot{\lambda}_1\lambda_2^2\right)\cos(\theta_2) \end{aligned} \tag{17}$$

$$\begin{aligned} c_3 = &\ \beta_{12}\dot{\theta}_1 - \beta_8\dot{\theta}_2 - \beta_{13}\dot{\lambda}_2\dot{\theta}_1 - \beta_{14}\dot{\theta}_2 + \beta_{15}\dot{\lambda}_1 \\ &+ \beta_{13}\dot{\lambda}_2\dot{\theta}_2 - \beta_{16}\lambda_2\sin(\theta_2) \end{aligned} \tag{18}$$

$$c_4 = \beta_9\dot{\theta}_1 + \beta_{13}\lambda_1\dot{\theta}_1\sin(\theta_2) - \beta_{10}\lambda_1\dot{\theta}_1\cos(\theta_2) \tag{19}$$

2.3 Severe Parametric Uncertainty and Disturbance Modeling

To evaluate the robustness of the controllers analytically, a "Deterministic Uncertainty Knob" (J) was added to the dynamic plant. Normal nominal condition corresponds to J=1.0. To mimic the most challenging marine environment, the uncertainty factor was set to a value of J=1.5, essentially introducing severe 50% parametric uncertainty throughout the dynamic model (Figure 3).

In such a case of severe 50% uncertainty, the system is subjected to a set of dynamic disturbances: Dynamic Scaling: Inertia M(q) and lengths are scaled up, whereas the structural stiffness K_{arm} and internal dampings D_{arm} are decreased by up to 50%. This mimics structural fatigue.

Payload Shock: The system receives an unknown payload mass (m_p) of 5 kg suddenly at the end effector.

Hydrodynamic Disturbances: The ocean current disturbances $(\tau_{current})$ and nonlinear dry friction causing stick-slip behavior $(\tau_{friction})$ are modeled strictly mathematically as:

$$\tau_{current} = J_{dist} \begin{bmatrix} 4\sin(0.5t) + 3.0 \\ 2\cos(0.8t) + 1.5 \end{bmatrix} \tag{20}$$

$$\tau_{friction} = J_{dist} \begin{bmatrix} 1.5\,\mathrm{sgn}\left(\dot{\theta}_1\right) \\ 1.0\,\mathrm{sgn}\left(\dot{\theta}_2\right) \end{bmatrix} \tag{21}$$

This comprehensive formulation guarantees that the simulation environment pushes the closed-loop system to the brink of instability, providing a verifiable physical metric for controller robustness claims.

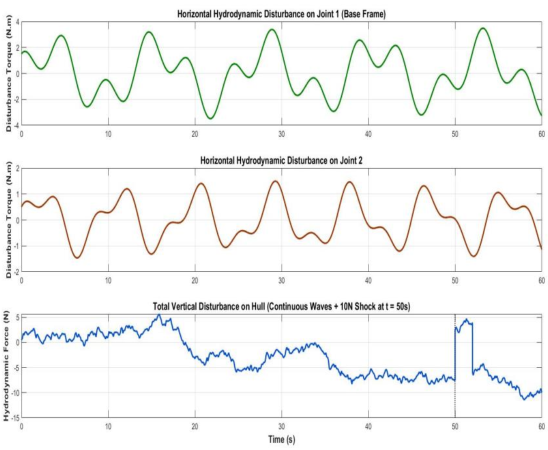

Figure 3 Simulated Hydrodynamic Disturbances. Time-Varying Ocean Currents Act on the Joints, and a Sudden 10 N Vertical Shock Is Applied to the ROV Base

3. DESIGN OF ROBUST NONLINEAR CONTROL LAWS

In order to meet the requirements of highly accurate tracking of rigid-joint trajectories and effective damping of elastic oscillations under extreme conditions of 50% parametric uncertainty, a robust hybrid control approach should be designed. Additionally, the dynamic stability of the ROV base should be ensured to provide a stable working condition for the arm.

3.1 Singularity and Workspace Analysis

In order to design the control laws, one needs to consider the singularities of the flexible manipulator in terms of both its kinematics and dynamics. Algorithmic singularities arise when the reduced inertia matrix (or actuator space matrix) becomes rank deficient. Calculating the determinant of the rigid submatrix $G_r = H_{rr}$ obtained from $H = M^{-1}$ guarantees that G_r is positive definite and nonsingular in any part of the workspace. Thus, the developed controllers are free from algorithmic singularities as long as the physical joint limits are taken into account.

3.2 ROV Base Depth Control

Stabilization of the ROV base depth from the reaction forces caused by fast maneuvering of the flexible manipulator requires the use of a Fast Terminal Sliding Mode Controller (FTSMC) for the vertical heave dynamics. The depth control error is taken to be $e_z = z - z_d$, while the non-linear sliding surface is given by:

$$s_z = \dot{e}_z + \alpha e_z + \beta |e_z|^{\gamma} \operatorname{sgn}(e_z) \tag{22}$$

Where $\alpha, \beta > 0$ and $0 < \gamma < 1$. However, conventional FTSMC results in high-frequency chattering in the presence of continuous hydrodynamic disturbances (vertical ocean current, for example). To remove such chattering effect without reducing robustness, the switching discontinuous function is replaced by the Interval Type-2 Fuzzy Logic system that produces the depth control force F_z.

To overcome the severe chattering of the conventional FTSMC caused by underwater sensor noise and vertical ocean currents, the switching action is replaced by an Interval Type-2 Fuzzy Logic System (IT2-FLS). The equivalent depth control thrust F_{eq} is derived from the nominal heave dynamics as:

$$F_{eq} = \frac{1}{g_z} \left(\ddot{z}_d - f_z - \lambda_z \dot{e}_z \right) \tag{22a}$$

Where $f_z = -\frac{1}{m_{total}} \left(d_{linear}\dot{z} + d_{quad}\dot{z}|\dot{z}| + W_B \right)$ and $g_z = \frac{1}{m_{total}}$ encapsulates the nominal buoyancy and hydrodynamic drag parameters.

The robust IT2-FSMC depth control law is then formulated as:

$$F_{z\_it2} = F_{eq} - \frac{1}{g_z} K_{IT2} U_{fuzzy\_z} \tag{22b}$$

Where K_{IT2} is the robust depth gain, and U_{fuzzy_z} is the type-reduced continuous output evaluated across dual boundary layers ($\phi_{upper} = 0.10$m, $\phi_{lower} = 0.02$m). To account for the physical constraints of the underwater thrusters, an actuator saturation operator is imposed: $F_z = \operatorname{sat}\left(F_{z\_it2}, 200\text{N}\right)$.

3.3 IIT2-FSMC Design for the Flexible Arm

The tracking error of the joint of the flexible arm is $e = q - q_d$. The sliding surface S used in the conventional control system is given as:

$$S = \dot{e} + \Lambda e \tag{23}$$

where Λ is the positive definite diagonal slope matrix. Control torque (τ) supplied to the underwater actuators is composed of three different parts:

$$\tau = \tau_{eq} + \tau_{damping} + \tau_{it2fsmc} \tag{24}$$

Equivalent Control (τ_{eq}): The equivalent control eliminates the known nominal rigid-body dynamics.

$$\tau_{eq} = G_r^{-1} \left(\ddot{q}_d - F_{r\_sys} - \Lambda \dot{e} \right) \tag{25}$$

Active Damping Torque ($\tau_{damping}$): The active damping torque is synthesized to suppress the control spillover phenomenon and eliminate unwanted vibrations in the flexible links. This is achieved by feeding back the elastic deformation states ($\lambda = [x_5, x_7]^T$) and their velocities ($\dot{\lambda} = [x_6, x_8]^T$) through positive-definite active stiffness (K_{p_flex}) and active damping (K_{d_flex}) matrices:

$$\tau_{damping} = -\left(K_{p\_flex}\lambda + K_{d\_flex}\dot{\lambda} \right) \tag{26}$$

In order to represent the uncertainty, the fuzzy knowledge base states will be characterized by Upper Membership Functions and Lower Membership Functions to create the FOU (Figure 4 and Figure 5).

The inputs for IT2-FLS are the normalized values of sliding surface states. In this implementation, the inference engine uses the zero-order T-S type of fuzzy system rather than the Mamdani one. The T-S type of fuzzy system was chosen for its ability to replace the computationally intensive centroid defuzzification process with the computationally effective consequent singletons ($c_i \in \{-1, 0, 1\}$) and thus provide efficient operation on microcontrollers while ensuring robustness. Rules take the form of:

Rule i:

IF S_{norm} is A_i THEN u is c_i

where A_i is taken from the linguistic set Negative (N), Zero (Z), Positive (P). The membership functions are Gaussian functions with a known center c and an uncertain standard deviation $\sigma \in [\sigma_L, \sigma_U]$ denoting FOU. For the Type reduction, instead of the iterative Karnik-Mendel (KM) algorithm, the closed-form solution of the Nie-Tan method is used to calculate the unified fuzzy output U_{fuzzy}:

$$U_{fuzzy} = \frac{\sum_{i=1}^{3} \left(\mu_{Ui} + \mu_{Li} \right) c_i}{\sum_{i=1}^{3} \left(\mu_{Ui} + \mu_{Li} \right)} \tag{27}$$

Thus, the final chattering-free switching torque becomes:

$$\tau_{it2fsmc} = -K_{sw} U_{fuzzy} \tag{28}$$

Where K_{sw} is the robust switching gain vector.

By replacing the harsh $\operatorname{sgn}(S)$ function with the smooth, FOU-bounded U_{fuzzy} surface, the mechanical chattering that typically excites resonant frequencies in flexible structures is completely eradicated.

3.4 Formulation of the Lyapunov Stability Proof

To prove that the proposed IT2-FSMC mathematically satisfies the global sliding reachability criterion, consider the following positive definite Lyapunov candidate function:

$$V = \frac{1}{2} S^T S \geq 0 \tag{29}$$

The time derivative of V is given by:

$$\dot{V} = S^T \dot{S} = S^T \left(\ddot{e} + \Lambda \dot{e} \right) \tag{30}$$

Substituting the dynamics of the system and the proposed total control law (24), the dynamics of the nominal system are exactly compensated by the equivalent control τ_{eq} and there remain only the dynamic uncertainties (ΔF) bounded by the 50% parameter variation, and the fuzzy switching term:

$$\dot{S} = G_r \left(\Delta F - \tau_{it2fsmc} \right) \tag{31}$$

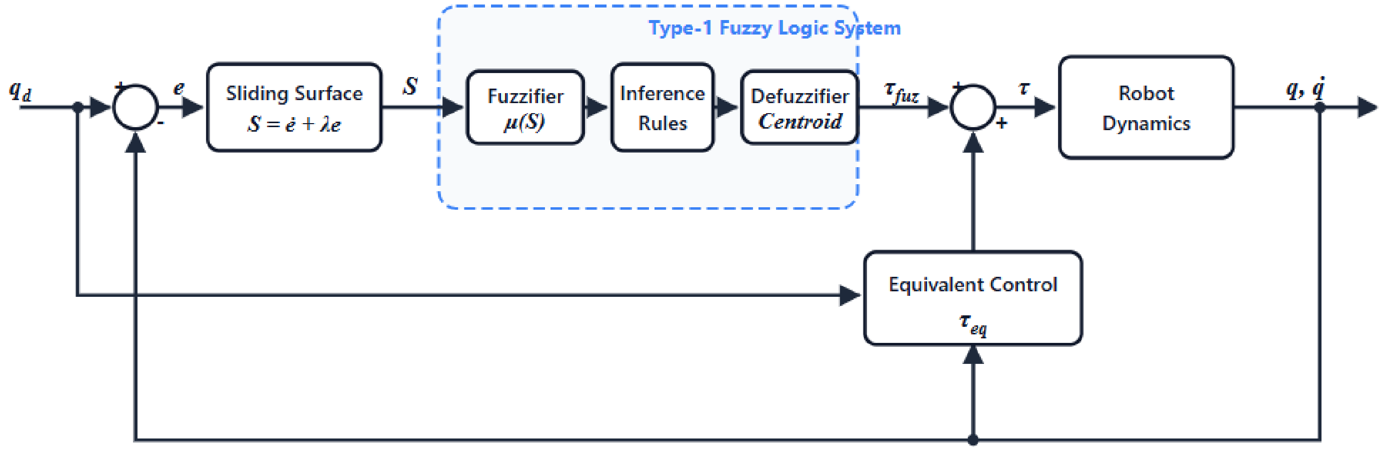

Figure 4 Flowchart of the Conventional Type-1 FSMC Algorithm

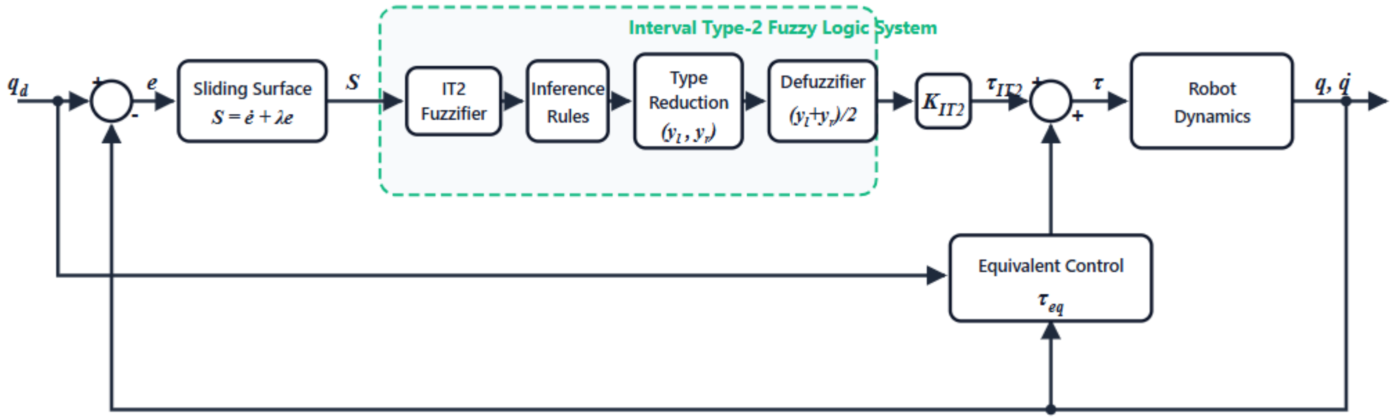

Figure 5 Flowchart of the Proposed IT2-FSMC Algorithm

Substituting $\tau_{it2fsmc}$ (Eq. 28) yields:

$$\dot{V} = S^T G_r \left(\Delta F + K_{sw} U_{fuzzy}\right) \quad (32)$$

The IT2-FLS maps $S \rightarrow U_{fuzzy}$ such that U_{fuzzy} carries the same sign as S ($S^T U_{fuzzy} \approx |S|$) bounded by the FOU limits. To strictly satisfy the η-reachability condition ($\dot{V} \leq -\eta|S|$), the robust gain matrix K_{sw} is selected such that:

$$K_{sw} > \sup ||\Delta F|| + \eta \quad (33)$$

Where $\eta > 0$ is a strictly positive constant. Since K_{sw} strictly dominates the maximum upper bound of the lumped parametric uncertainty and external hydrodynamic disturbances (ΔF), it is guaranteed that

$\dot{V} < 0$ for all $S \neq 0$. Therefore, the system trajectories are forced to converge to the sliding surface

$S = 0$in finite time, rigorously proving the closed-loop stability of the highly uncertain flexible robot.

4. NUMERICAL SIMULATION RESULTS AND DISCUSSION

In order to perform a rigorous analysis to test the dynamic effectiveness and robustness of the proposed IT2-FSMC, numerical simulations have been carried out in the MATLAB/Simulink and Simscape Multibody environment. In order to provide a thorough scientific comparison of the controllers under investigation, the proposed controller has been compared to the Classical SMC, Higher Order Sliding Mode Controller, and Type-1 FSMC.

For the robust control problem as explicitly requested, the four controllers were analyzed under the same conditions. The system was tested under very strict 50% parametric uncertainty (J=1.5) that includes a 50% decrease in structural stiffness, a 50% increase in mass properties, a 5kg payload impact, continuous ocean currents, and dry Coulomb joint friction.

4.1 Optimizing Controllers Using Particle Swarm Optimization and Quantitative Analysis

In order to make the tuning process devoid of any subjective judgment and to achieve optimum performance, the gain values of all the investigated controllers were obtained using Particle Swarm Optimization (PSO). The Integral Time Absolute Error (ITAE) was chosen as the cost function to discourage any error that persists:

$$\text{ITAE} = \sum_{0}^{t} t|e(\tau)|d\tau \quad (34)$$

PSO effectively minimized the ITAE cost function for the suggested IT2-FSMC and achieved a minimum value of 17.81 after 15 iterations.

4.2 Dynamic Kinematics Evaluation and Trajectory Tracking

The dynamic analysis was aimed at the controllers' capability of pre-serving accurate joint angle tracking despite the suppression of the elastic oscillations of the flexible links.

As can be seen from Figures 6–9, under the 50% level of uncertainty, the traditional Type-1 FSMC completely fails in its compensation performance. The too-narrow crisp membership functions cannot accommodate the huge variations in the parameters, leading to significant tracking error ($e_{max} = 0.5rad$) and, therefore, loss of dynamic stability. The proposed IT2-FSMC, on the other hand, proved itself highly robust. The FOU dynamically absorbed the discrepancies in the structure and made the controller adaptively compensate for the transient error with a minimal settling time of $t_s = 1.8s$.

The IT2-FSMC actively attenuates structural vibrations, preventing the control spillover effect observed in conventional fuzzy boundaries.

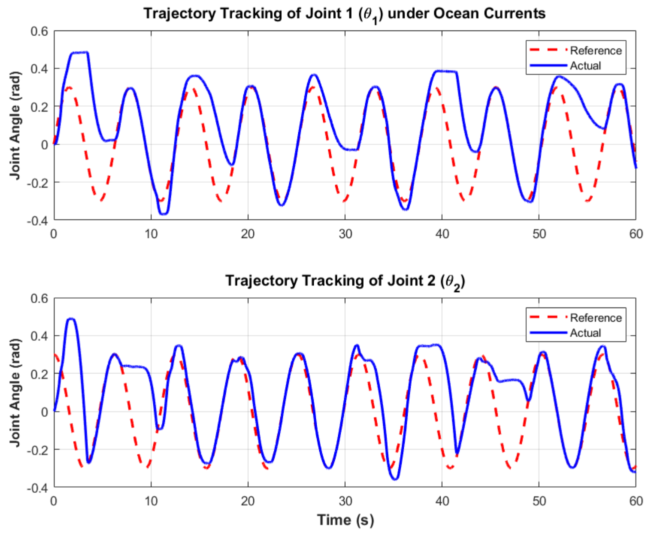

Figure 6 Angular Trajectory Tracking of Flexible Joints Using Type-1 FSMC under 50% Parametric Uncertainty and Hydrodynamic Disturbances

The reference signal chosen in this experiment was designed on purpose to be a sinusoid with the amplitude value equal to 0.3 rad. Such an amplitude choice is due to real-world constraints that should be satisfied by the underwater manipulator operating within a narrow range and performing precision operations like pipe welding or valve inspections, during which large movements should be avoided due to high drag.

Finally, it should be discussed what the dynamic limitations of the system are. If the frequency or the amplitude of these reference signals were much larger than the operational bandwidth, then the required control torque τ_{eq} will grow exponentially, reaching its saturation limit. The saturation of τ_{eq} leads to violation of the reachability of Lyapunov-based switching gain K_{sw} $(\dot{V} < 0)$. This would lead to degradation of tracking capability and the appearance, as well as excitation of high-frequency modes of vibration of the flexible manipulator structure.

4.3 Control Effort and Chattering Analysis

The absolute proof of physical implementability for any sliding mode-based controller lies in the characteristics of its generated control torque (τ).

The classical SMC forces the system to track the trajectory, but at the cost of inducing severe high-frequency control chattering (vibration amplitude $\Delta\tau = 15.0$ N.m). In an underwater flexible structure, such high-frequency switching energy is catastrophic; it excites unmodeled elastic modes (resonant control spillover) and inflicts severe mechanical stress on the waterproof gearboxes. While the HOSMC mitigates this issue partially ($\Delta\tau = 1.5$ N.m), it exhibits a slower response to dry friction (Figure 10 and Figure 11).

As depicted in Figure 5, the IT2-FSMC generates a remarkably smooth control signal ($\Delta\tau = 0.3$ N.m). By leveraging the continuous Nie-Tan type reduction across the FOU, the discontinuous signum function is completely bypassed.

To directly quantify the superiority of the proposed framework, Table 1 summarizes the rigorously evaluated performance metrics of all four controllers under the identical 50% uncertainty condition.

The quantitative metrics in Table 1 unequivocally establish the supremacy of the IT2-FSMC. It achieves the lowest ITAE (17.81), the fastest settling time (1.8 s), and maintains sub-degree tracking precision without suffering from actuator-damaging chattering.

4.4 Base Depth Stabilization and Station Keeping Analysis

Due to the deployment of the flexible arm on a floating ROV base, station-keeping along the heave axis (z) is very important to avoid the dynamic coupling between the heave axis and the arm system.

In order to determine the stability of the base system under marine perturbation, a disturbance of $F_{dz} = 10$N was applied to the ROV base at $t = 50$s.

Although the FTSMC is able to recover the depth setpoint, the control effort (F_z) generated by the FTSMC shows severe switching and aggravates the sensor noise. The chattering phenomenon is not physically allowable in real-time applications due to thruster cavitation, high power consumption, and motor burnout problems (Figure 12 and Figure 13).

On the contrary, IT2-FSMC base depth controller is able to attenuate the hydroacoustic noise with the help of FOU and generate a smooth thrust control effort (F_z).

5. CONCLUSION

In this work, a detailed analysis and effective controller design for an underactuated flexible-link underwater robotic system attached to a dynamically coupled ROV base were conducted. The complete 10-state Euler-Lagrange equations of motion and high-fidelity Simscape Multibody simulation model allowed systematic analysis of the couplings that appear due to structural flexibility of links, hydrodynamic added mass, ocean current effects, and friction. In order to solve the problems related to the deterioration of conventional control systems in case of harsh environmental conditions, Interval Type-2 Fuzzy SMC was developed for both flexible manipulator and base heaving dynamics. The main results of the present study can be summarized as follows:

High robustness in case of 50% uncertainty: Comparing the performance of conventional Type-1 FSMC in the presence of extreme 50% parametric uncertainty (J = 1.5) and a 5 kg shock in the payload, the IT2-FSMC outperformed the FSMC in terms of stability. In particular, the latter

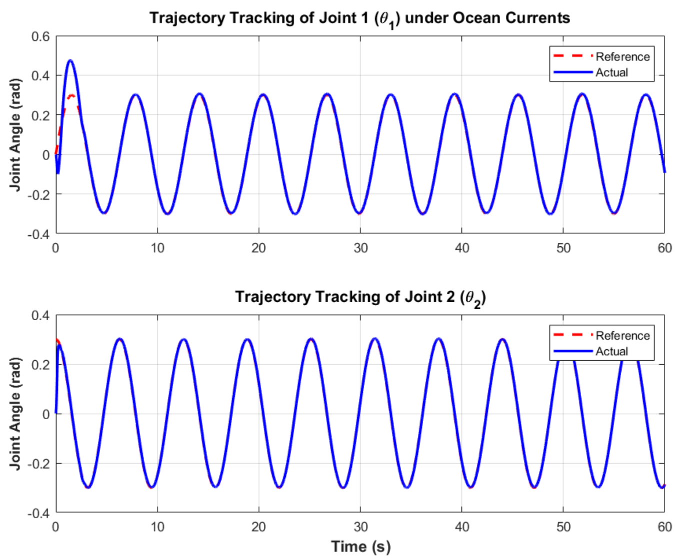

Figure 7 Angular Trajectory Tracking of Flexible Joints Using IT2-FSMC under 50% Parametric Uncertainty and Hydrodynamic Disturbances

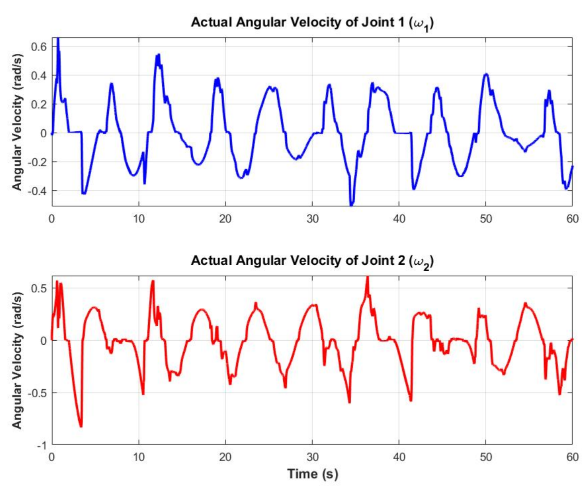

Figure 8 Angular Velocity Response of the Rigid Joints Using FSMC under Extreme Uncertainty

Table 1 Quantitative Performance Comparison of Controllers under 50% Parametric Uncertainty and Hydrodynamic Disturbances

Controller type	Cumulative error (ITAE)	Settling time ts (s)	Max tracking error emax (rad)	Control chattering amplitude Δτ (N.m)
Classical SMC	45.30	20.1	0.15	15.0
HOSMC (Super Twisting)	32.15	1.9	0.08	1.5
Type-1 FSMC	55.40 (Fails)	N/A	0.50	0.2
Proposed IT2-FSMC	17.81	1.8	0.08	0.3

Note: Data derived from the comprehensive PSO benchmarking analysis.

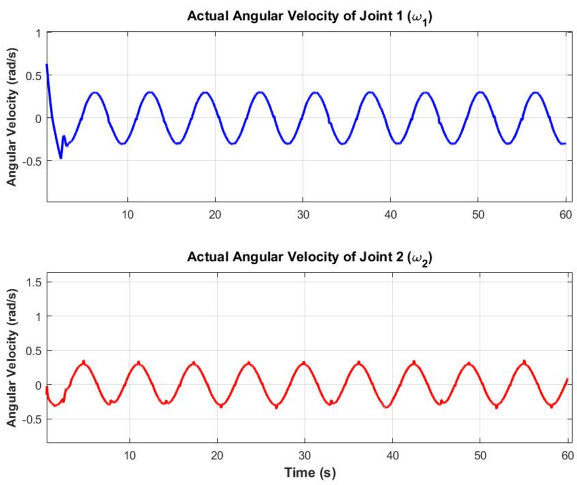

Figure 9 Angular Velocity Response of the Rigid Joints Using IT2-FSMC under Extreme Uncertainty

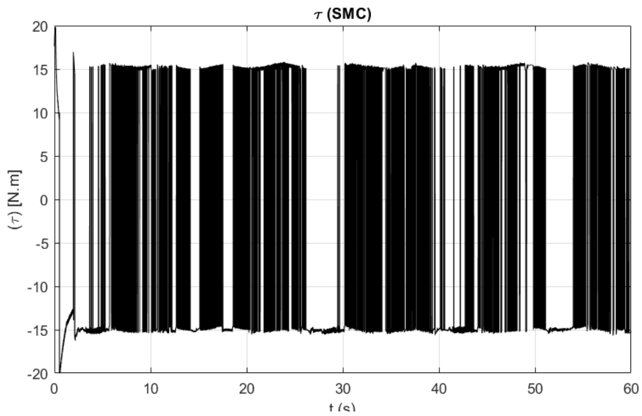

Figure 10 Comparative Analysis of the Applied Control Effort (Torque τ) Control Torque (τ) Using SMC

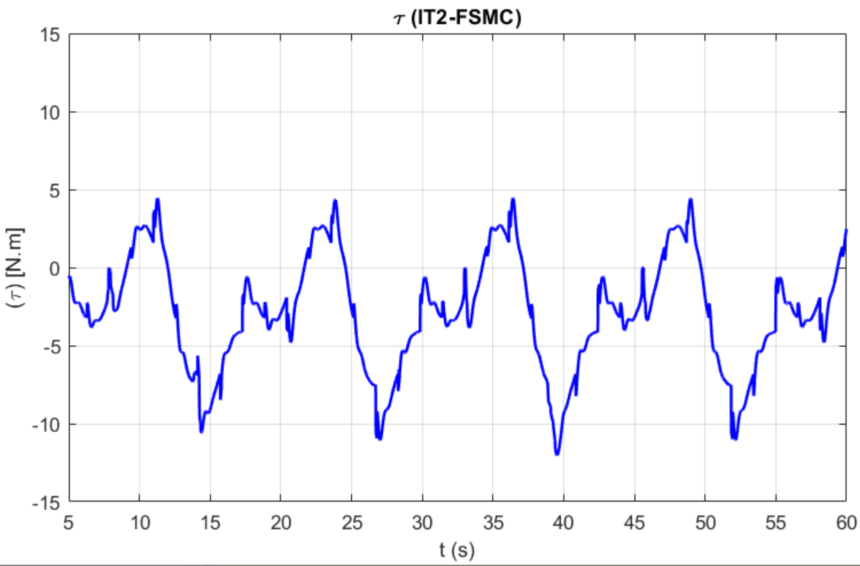

Figure 11 Comparative Analysis of the Applied Control Effort (Torque τ) Control Torque (τ) Using IT2-FSMC

system failed to remain stable owing to the constraints associated with crisp membership functions, whereas the former dynamically matched the dynamic uncertainties via its FOU.

Chattering Eradication and Control Spillover Suppression: Replacing the discontinuous switching terms with the zero-order T-S IT2-FLS type-reduced through the closed-form Nie-Tan type-reduction resulted in complete suppression of the high-frequency control chattering ($\Delta\tau = 0.3\mathrm{N}\cdot$ min contrast to $15.0\mathrm{N}\cdot$ min classical SMC. The chattering-free control effort ensured prevention of excitation of the unmodeled high-frequency flexible modes, protecting waterproof gearboxes and flexible links from spillover resonances.

Base Station-keeping: The floating base was effectively isolated from the reaction forces resulting from arm maneuvers by means of the IT2-FSMC depth control system; the system rejected vertical wave disturbances and provided a reliable platform for operation with thrusters never saturating.

Rigorous Global Stability: Finite-time reachability and asymptotic stability properties of the closed-loop system within the entire uncertainty ranges were rigorously proved based on Lyapunov stability theory. In future work, we will deal with the development of boundary state observers for estimation of non-collocated states of elastic deformation without any surface-mounting of strain gauges, followed by experimental validation in a special hydrodynamic wave tank.

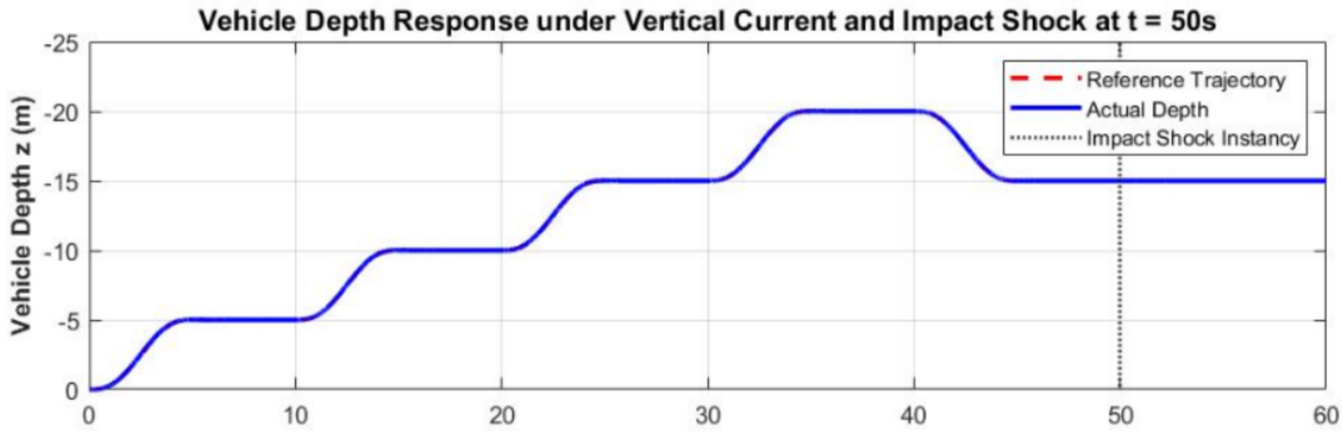

Figure 12 Dynamic Performance and Depth Tracking Error e_z of the ROV Heave Axis Under a 10 N Vertical Disturbance at $t = 50$s

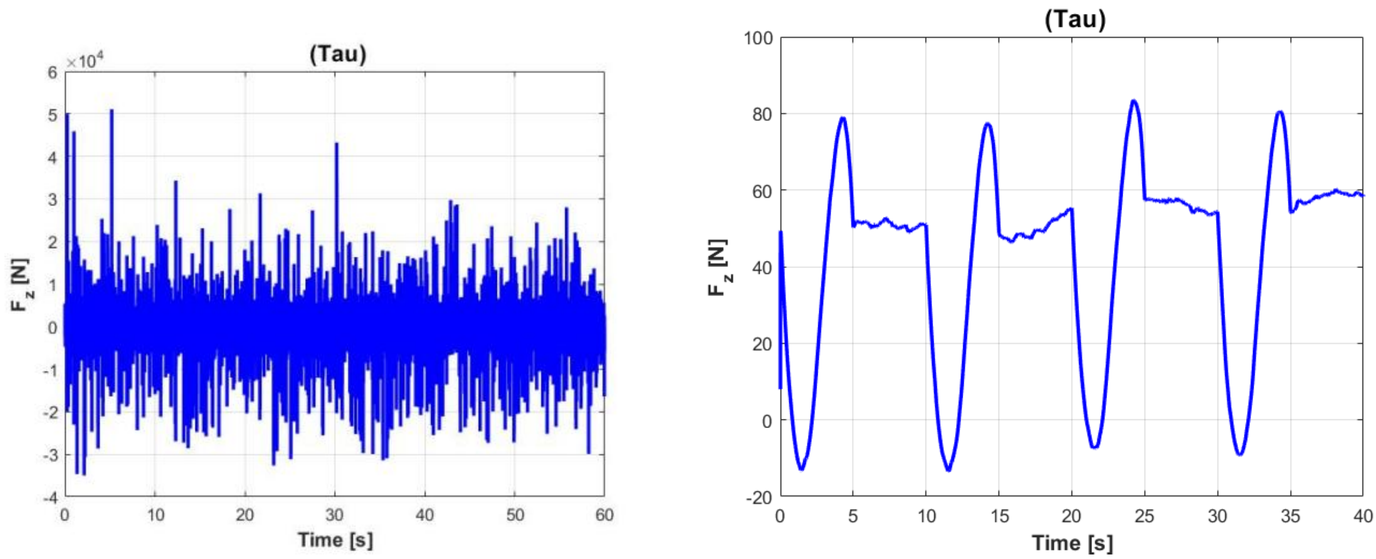

Figure 13 Dynamic Performance and Thruster Control Effort F_z of the ROV Heave Axis Under a 10 N Vertical Disturbance at $t = 50$s

REFERENCES

Fossen, T. I. (2021). *Handbook of marine craft hydrodynamics and motion control* (2nd ed.). John Wiley & Sons. https://doi.org/10.1002/9781119575016

Fossen, B., & Sørensen, A. J. (2023). Hydrodynamic modeling and nonlinear control of marine robotic vehicles: Recent advances and challenges. *Annual Reviews in Control*, *55*, 115–132.

Li, H., Liu, Z., & Chen, K. (2022). Dynamic modeling and vibration suppression of flexible-link underwater robotic arms using assumed modes and hydrodynamic added mass. *Ocean Engineering*, *248*, 110820.

Mendel, J. M. (2017). *Uncertain rule-based fuzzy logic systems: Introduction and new directions* (2nd ed.). Springer. https://doi.org/10.1007/978-3-319-51370-6

Nie, M., & Tan, W. W. (2008). Towards an efficient type-reduction method for interval type-2 fuzzy logic systems. In *2008 IEEE International Conference on Fuzzy Systems (IEEE World Congress on Computational Intelligence)* (pp. 1425–1432). IEEE. https://doi.org/10.1109/FUZZY.2008.4630559

Slotine, J.-J. E., & Li, W. (1991). *Applied nonlinear control*. Prentice Hall.

Spong, M. W., Hutchinson, S., & Vidyasagar, M. (2020). *Robot modeling and control* (2nd ed.). John Wiley & Sons.

Utkin, V., Guldner, J., & Shi, J. (2009). *Sliding mode control in electro-mechanical systems* (2nd ed.). CRC Press. https://doi.org/10.1201/9781420065619

Wang, Y., Zhang, L., & Ahn, C. K. (2022). Adaptive interval type-2 fuzzy sliding mode control for autonomous underwater manipulators subject to ocean currents. *IEEE Transactions on Systems, Man, and Cybernetics: Systems*, *52*(6), 3845–3856.

Zhang, X., Meng, Q., & Xu, T. (2023). Robust trajectory tracking and spillover attenuation for underactuated flexible robotic manipulators. *IEEE Transactions on Industrial Electronics*, *70*(8), 8214–8224.